

Ultrafast terahertz probes of interacting dark excitons in chirality-specific semiconducting single-walled carbon nanotubes

Liang Luo, Ioannis Chatzakis[†], Aaron Patz, Jigang Wang^{*}
*Department of Physics and Astronomy and Ames Laboratory-U.S. DOE,
Iowa State University, Ames, Iowa 50011, USA.*

(Dated: June 16, 2022)

Ultrafast terahertz (THz) spectroscopy accesses the *dark excitonic ground state* in resonantly-excited (6,5) SWNTs via internal, direct dipole-allowed transitions between lowest lying dark-bright pair state ~ 6 meV. An analytical model reproduces the response which enables quantitative analysis of transient densities of dark excitons and unbound *e-h* plasma, oscillator strength, transition energy renormalization and dynamics. Stable quasi-1D many-exciton states rapidly emerge even with increasing off-resonance photoexcitation and evolve uniquely from a predominant dark exciton population to complex phase-space filling of both dark and bright pair states, distinctly different from dense 2D and 3D excitons characterized by the ionization to free carriers and slow formation.

A major challenge both in fundamental quasi-one-dimension (quasi-1D) physics of single-walled carbon nanotubes (SWNTs) and for their technological development is to detect, understand and control exciton multiplexes. On one hand, SWNT excitons, with large binding energies of 100s of meV, naturally arise from strong quantum confinement and reduced screening of electron-hole (*e-h*) pairs [1, 2]. Their internal structure is characterized, in a 1D hydrogen atom-like description, by a center-of-mass momentum K and by internal quantum numbers (designated here as $1s$, $2s$, $2p\dots$). These strong excitonic behaviors manifest themselves in extensive static/ultrafast optical interband absorption/emission spectra in individually separated SWNTs, which are stable even in the presence of unbound *e-h* carriers from residual tube aggregation and/or metallic tubes [3–6]. On the other hand, unlike the hydrogen atom, the correlated *e-h* pairs in SWNTs evolve in a “modified vacuum” with exotic, chiral symmetry arising from the underlying graphene lattice that gives two-fold degeneracy at K and K' points. Coulomb interaction splits such “doubling” into odd (u) and even (g) symmetry states entailing a series of bright and optically-forbidden, dark exciton pairs, including the lowest $1s(u)$ and $1s(g)$ [7, 8] [Fig. 1(a)]. Thus far, the dark ground state $1s(g)$, hidden from both single- and two-photon optical interband transitions, is still largely unexplored.

While magneto-optics and light scattering measurements established the existence of dark excitons in SWNTs [9–11], the search for possible dipole-allowed, lowest transitions $1s(g)\rightarrow 1s(u)$ remains open. Many key properties have yet to be characterized, including its oscillator strength. Particularly, as these linear probes do not depend critically on quasi-particle/exciton interaction and the associated fast dynamics, they provide little insight into many-exciton interacting states, which are characterized by the co-existence of both the dark & bright excitons, and complex interplay between excitons and *e-h* plasma. Exactly these aspects govern the radiative lifetime and photoluminescence efficiency, key for

SWNT-based optoelectronic applications [7, 12]. The lack of quantitative probes and scarce ultrafast measurements for dark states seriously limit their thorough understandings and perspectives of exploring related novel quantum phenomena, e.g., the excitonic Bose-Einstein condensate and macroscopically-ordered phase [13].

Selective optical pump and THz probe technique represents a versatile spectroscopy tool that is extremely relevant for *quantitative* study of dark excitons. THz pulses directly couple the $1s(g)\rightarrow 1s(u)$ transitions [arrows, Fig. 1(a)]. Being independent of K , THz pulses measure genuine dark exciton population across momentum space, while the available interband optical probes, due to symmetry and momentum conservation, only detect a subset of excitons near $K=0$. Additionally, the simultaneously-obtained ultrafast conductivity and dielectric function *quantitatively* follow the dynamic evolution of both the excitons and *e-h* plasma. Moreover, the capability of resonant and off-resonant excitations by tuning the pump photon energy enables, among others, the study of excitons in single chirality tube and of exciton-plasma interaction. These critical aspects for dark exciton studies are absent in prior THz experiments of SWNTs, which largely focus on the non-Drude conductivity and low energy absorption band centered ~ 4 THz [14–16].

In this Letter, we reveal lowest lying dark excitons and their interacting states in semiconducting SWNTs. With resonant excitation to the (6,5) E_{22} interband transition at low temperature, transient THz spectra evidence strong photoinduced absorption centered ~ 6 meV, whose transition energy, pump photon and temperature dependence, and dynamics manifest the observation of the $1s(g)\rightarrow 1s(u)$ transition. The THz response is reproduced by an analytical model that quantitatively measures the transient densities of excitons and unbound *e-h* carriers. The resonant pumping generates mostly excitons and, at low fluence, allows to determine the oscillator strength $f_{g\rightarrow u}^{1s} \approx 0.79$, while off-resonant excitation significantly increases the amount of unbound carriers, which shifts the THz resonance. Most intriguingly, the $1s(g)\rightarrow 1s(u)$

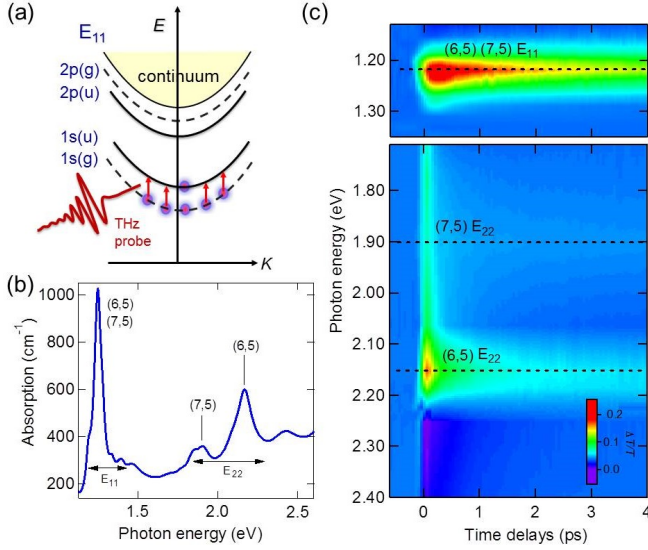


FIG. 1. (Color online) (a) Schematic of two-particle e - h pair dispersion, illustrating the lowest lying $1s(g) \rightarrow 1s(u)$ intra-excitonic transitions (arrows) resonantly probed by THz pulses. Absorption spectra (b) and time/spectral-resolved differential transmission $\Delta T/T$ after 1.55 eV photoexcitation (c) of the SWNT sample at $T=300$ K.

oscillator signals emerge quasi-instantaneously even with increasing off-resonance photoexcitation and drop significantly above $\sim 130 \mu\text{J cm}^{-2}$, at which the intra-excitonic resonances are *still stable with little shift or broadening*. This appears to be distinctly different from dense 2D and 3D excitons that are characterized by ionization to free carriers and slow formation [17]. Robust transient quasi-1D many-exciton states, instead, uniquely evolve from a predominant dark exciton population to complex phase-space filling of both dark and bright pair states.

We study Co-Mo-catalyst grown SWNTs of mainly (6,5) and (7,5) chiralities embedded in a freestanding $50 \mu\text{m}$ Sodium Dodecylbenzenesulfonate (SDBS) film through drying a D_2O solution of SDBS-dispersed SWNTs (supplementary). The SDBS both ensures wide transparency of the polymer matrix in THz range and also serves as surfactant to effectively reduce SWNT bundles [18]. The absorption spectrum in Fig. 1(b) exhibits the distinct E_{11} and E_{22} quantized interband absorption peaks of dominant (6,5) and (7,5) chiralities, each associated with substantially prolonged relaxation times and significantly enhanced photobleaching, as shown in the differential transmission spectra [Fig. 1(c)]. These observations are consistent with the extensive interband studies of high-quality chirality-enriched SWNT samples at visible and near-infrared spectral regions, which are explained by the joint effects of resonantly-enhanced radiative lifetime and exciton Auger process [3, 4].

Our optical pump THz probe spectroscopy setup is driven by a 1 kHz Ti:Sapphire regenerative amplifier with

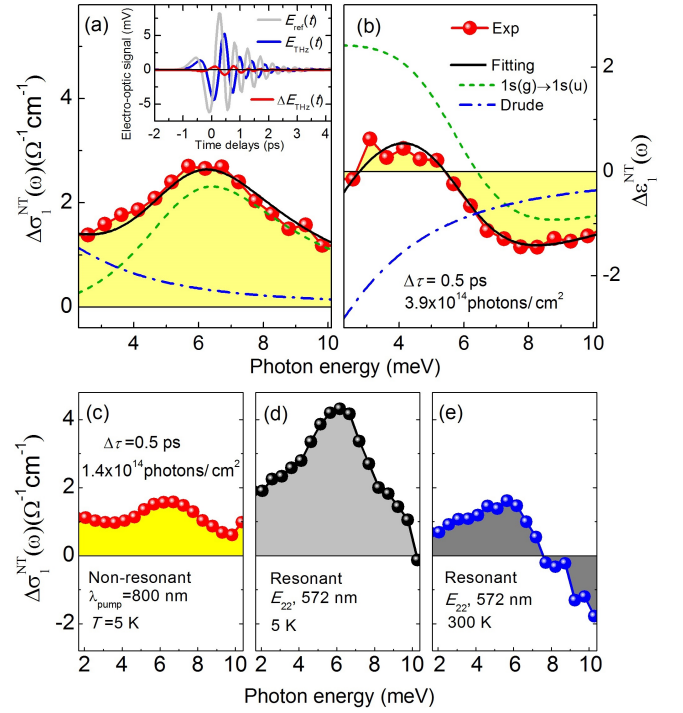


FIG. 2. (Color online) Ultrafast THz spectra of $\Delta\sigma_1^{\text{NT}}(\omega)$ (a) and $\Delta\epsilon_1^{\text{NT}}(\omega)$ (b) (red dots), measured at pump-probe delay $\Delta\tau=0.5$ ps after 1.55 eV pumping. Thick line is the fit using the analytical model, Eq.(1), which is sum of the $1s(g) \rightarrow 1s(u)$ excitonic (dashed green) and unbound e - h responses (dash-dotted blue) (main text). Inset: THz fields transmitted through reference (gray), unexcited sample (blue), and excited sample (red, $\times 15$). Comparison of photoinduced $\Delta\sigma_1^{\text{NT}}(\omega)$ at $\Delta\tau=0.5$ ps and under excitation density $1.4 \times 10^{14} \text{ cm}^{-2}$: (c) Off-resonant pumping at 1.55 eV and $T=5\text{K}$; (d) on-resonant pumping at 2.17 eV and $T=5\text{K}$; (e) on-resonant pumping at 2.17 eV and $T=300\text{K}$.

40 fs pulse duration and 800 nm center wavelength. One part of the output is to pump the frequency-doubled, near-IR optical parametric amplifier which resonantly excites the E_{22} transition of the (6,5) tubes at 2.17 eV. Another part generates and detects phase-locked THz field transients, used as a probe, via optical rectification and electro-optic sampling in 1 mm thick $\langle 110 \rangle$ ZnTe crystals. The THz fields in time domain are measured, shown in the inset of Fig. 2(a), for transmission through reference (a clear aperture in our case) $E_{\text{ref}}(t)$ (gray), unexcited sample $E_{\text{THz}}(t)$ (blue), and its pump induced change $\Delta E_{\text{THz}}(t)$ after a pump-probe delay $\Delta\tau=0.5$ ps (red). Through the fast Fourier transformation and Fresnel equation, the frequency dependent complex-valued dielectric function for unexcited sample $\tilde{\epsilon}(\omega)$ and its pump induced transient change $\Delta\tilde{\epsilon}(\omega, \Delta\tau) = \tilde{\epsilon}_{\text{excited}}(\omega, \Delta\tau) - \tilde{\epsilon}(\omega)$ are obtained [19]. The corresponding conductivity can be calculated by $\tilde{\sigma}(\omega) = i[1 - \tilde{\epsilon}(\omega)]\omega\epsilon_0$. Effective medium theory is applied to obtain the SWNT dielectric

function from the experimental data (supplementary). The full THz dielectric response is expressed as the real part of the conductivity, $\sigma_1^{\text{NT}}(\omega)$, and of the dielectric function, $\varepsilon_1^{\text{NT}}(\omega)$, which measures the absorbed power and the out-of-phase, inductive response, respectively.

Representative ultrafast THz responses $\Delta\sigma_1^{\text{NT}}(\omega)$ and $\Delta\varepsilon_1^{\text{NT}}(\omega)$ are shown in Figs. 2(a)-2(b) (red dots) at $\Delta\tau=0.5$ ps and $T=5$ K, after 1.55 eV pumping with photon density 3.9×10^{14} cm $^{-2}$. A strong photo-induced absorption appears in $\Delta\sigma_1^{\text{NT}}(\omega)$ within the time resolution with a broad, resonant spectral shape centered at ~ 6 meV and a dispersive zero crossing occurs in $\Delta\varepsilon_1^{\text{NT}}(\omega)$ at slightly lower photon energy. These two features are characteristic of a well-defined driven THz oscillator while the shift between their spectral positions and the non-vanishing conductivity, albeit small, at the lowest probe energy ~ 2 meV indicate additional low-frequency spectral weight, in the form of a coexisting unbound e - h plasma as discussed later. We emphasize three key facts to assign this resonance mainly from the $1s(g) \rightarrow 1s(u)$ transition of (6,5) tubes. First, resonant photoexcitation of the (6,5) interband E_{22} excitonic transitions at 2.17 eV, shown in Fig. 2(d), leads to significant enhancement of the transient THz resonance ~ 6 meV, e.g., more than three times larger than the 1.55 eV off-resonant excitation [Fig. 2(c)], for the same excitation photon density $n=1.4 \times 10^{14}$ cm $^{-2}$ per pulse. This clearly shows the excitonic origins of the THz resonance in (6,5) tubes. Second, raising the initial lattice temperature to $T=300$ K [Fig. 2(e)] diminishes the resonance as compared to $T=5$ K [Fig. 2(d)], for the same resonant excitation. Third, the resonance occurs in the transparent region of the unexcited sample and is close to the $1s(g) \rightarrow 1s(u)$ transition energy of (6,5) tubes indirectly extrapolated in high field magneto-optical studies [9, 10].

For a quantitative analysis, a theoretical model is used to reproduce the experimentally determined complex THz dielectric functions. The model consists of two components: the THz dielectric function of the intra-excitonic transitions $\varepsilon_{g \rightarrow u}^{1s}(\omega)$ plus a Drude term of unbound e - h plasma $\varepsilon_{eh}(\omega)$

$$\varepsilon^{\text{NT}}(\omega) = \varepsilon_{g \rightarrow u}^{1s}(\omega) + \varepsilon_{eh}(\omega) = \left[\varepsilon_{\infty} + \frac{F_{g \rightarrow u}^{1s}}{(\omega_{g \rightarrow u}^{1s})^2 - \omega^2 - i\omega\Gamma} \right] - \frac{\omega_p^2}{\omega^2 + i\omega\gamma}. \quad (1)$$

For the first component (dashed green), $F_{g \rightarrow u}^{1s}$ denotes effective transition strength of the intra-excitonic $\omega_{g \rightarrow u}^{1s}$ resonance as $F_{g \rightarrow u}^{1s} = f_{g \rightarrow u}^{1s} \cdot (\Delta\omega_p^2)_{g \rightarrow u}^{1s}$, where f is the oscillator strength and $\omega_p^2 = ne^2/\varepsilon_0 m$. The $\Delta\omega_p^2$ term, thereby, measures the population difference Δn between the lowest dark and bright pair states [Fig. 1(a)], i.e., $\Delta n_X = n_g^{1s} - n_u^{1s}$. The second, Drude component (dash-dotted blue) is added with ω_p^2 proportional to the density of unbound e - h density n_{eh} . ε_0 and ε_{∞} are the vacuum and background permittivity, and e and m are the elec-

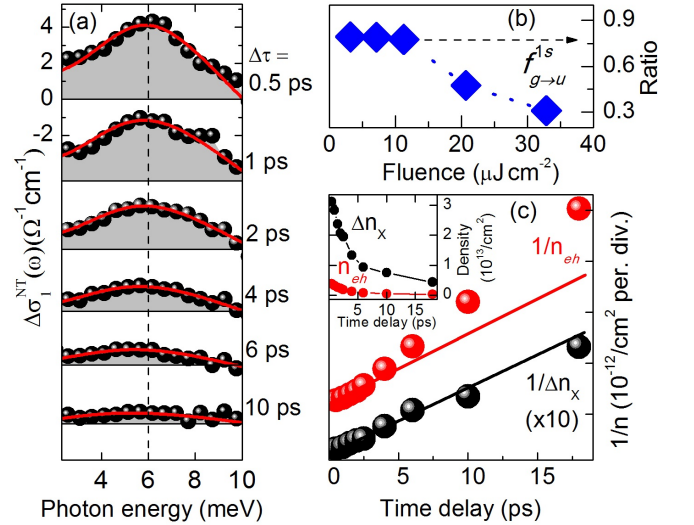


FIG. 3. (Color online)(a) photo-induced conductivity changes $\Delta\sigma_1^{\text{NT}}(\omega)$ (black dots) at several pump-probe delays after resonant (6,5) E_{22} excitation at 2.17 eV and $T=5$ K. The model described in text reproduces the experimental results (red lines). Dash line marks the peak positions. (b) The ratio $R = F_{g \rightarrow u}^{1s} \cdot (\varepsilon_0 m / e^2) / (n_{\text{ph}} - n_{eh})$ as a function of fluence. (c) The reciprocal of exciton (Δn_X) and unbound e - h (n_{eh}) carrier densities as a function of time delay together with fitting. The traces are vertically offset for clarity. Inset: temporal decay of Δn_X and n_{eh} .

tron charge and the effective exciton (or electron) mass obtained from [20]. Such composite THz response model (solid black lines) provides an excellent agreement with the low temperature experiment (red dots) in Figs. 2(a)-2(b) by varying the $\omega_{g \rightarrow u}^{1s}$ and $F_{g \rightarrow u}^{1s}$, carrier density n_{eh} , and the exciton (carrier) broadening Γ (γ). The best fit are strongly restrained by the requirement of simultaneously satisfying both dielectric responses $\Delta\sigma_1^{\text{NT}}(\omega)$ and $\Delta\varepsilon_1^{\text{NT}}(\omega)$, over a broad spectral range, and by the distinctly different spectral shapes of the excitonic oscillator and Drude carriers. Note that the model described above starts to deviate from the experimental spectra at high temperature or large exciton density, e.g., the negative $\Delta\sigma_1^{\text{NT}}(\omega)$ in the 300 K trace in Fig. 2(e). This can be fully resolved by an additional contribution from a photo-bleaching of the absorption band centered ~ 4 THz, which were extensively described in the prior study [14] (supplementary) and discussed later.

The intraexcitonic $1s(g) \rightarrow 1s(u)$ probe *quantitatively* unveils the dark e - h pair correlation after resonant photoexcitation of (6,5) SWNTs. Fig. 3(a) presents in detail of ultrafast THz conductivity spectra $\Delta\sigma_1^{\text{NT}}(\omega)$ for various time delays $\Delta\tau$ after the E_{22} photoexcitation at 2.17 eV. Pump fluence is $48 \mu\text{J cm}^{-2}$ and $T=5$ K. The transient spectra are characterized by the $\omega_{g \rightarrow u}^{1s}$ resonance that retains its shape as the amplitude decays with time. The resonance peaks, marked by the dash line, exhibit no

noticeable shift. The results can be fitted very well by the model described above (red lines) where optimum values of the effective transition strength $F_{g \rightarrow u}^{1s}$ and unbound $e-h$ density n_{eh} are obtained. In order to further determine the exciton density $\Delta n_X = (F_{g \rightarrow u}^{1s}/f_{g \rightarrow u}^{1s}) \cdot (\epsilon_0 m/e^2)$, the oscillator strength f is needed for the $1s(g) \rightarrow 1s(u)$ transition which has never been determined before. This can be directly obtained via fluence dependence. Fig. 3(b) plots the ratio $R = F_{g \rightarrow u}^{1s} \cdot (\epsilon_0 m/e^2)/(n_{ph} - n_{eh})$ as a function of fluence down to $3 \mu\text{J cm}^{-2}$, where n_{ph} is the actual absorbed photon density after taking into account the reflection and transmission of the pump beam in the optical path. This ratio, with sufficiently weak photoexcitation, will converge to $f_{g \rightarrow u}^{1s}$ since nearly all photo-generated E_{22} excitons will populate in the dark ground state $1s(g)$ during the THz pulse and $\Delta n_X \approx n_{ph} - n_{eh}$. This condition is ensured due to fast inter-subband E_{22} -to- E_{11} relaxation ~ 40 fs [21], low transient excitonic temperature and strongly limited exciton-exciton annihilation (EEA) in dilute exciton gas [22]. Indeed, the ratio shown in Fig. 3(b) exhibits strong pump power dependence and, with decreasing fluence below $\sim 10 \mu\text{J cm}^{-2}$, converges to a constant $f_{g \rightarrow u}^{1s} \approx 0.79$. Increasing pump fluence to 10s of $\mu\text{J cm}^{-2}$ leads to a significant drop of the ratio, which can be attributed to efficient EEA that lowers the photon-exciton conversion efficiency.

The obtained density Δn_X and its relaxation dynamics (black dots) are well described by a bimolecular decay shown in Fig. 3(c). Although it exhibits a highly non-exponential profile over ps time scales, shown in the inset, a reciprocal plot of $1/\Delta n_X(t)$, instead, yields a simple straight line, i.e., $1/\Delta n_X(t) \sim \beta t$ (black dots), which is the hallmark of the bimolecular decay given by $\frac{d}{dt} \Delta n_X(t) = -(1/2)\beta \Delta n_X^2(t)$ with decay rate of sheet density $\beta = 2.3 \times 10^{-14} \text{ cm}^2 \text{ ps}^{-1}$ [3]. The $1/n_{eh}(t)$ decay (red dots), on the contrary, show large variation from the bimolecular behavior, which further underscores the excitonic origin of the Δn_X response. Furthermore, the strong similarity between the $\Delta n_X(t)$ decay and firmly established exciton kinetics in SWNTs also indicates that most excitons populate in the $1s(g)$ ground state and $\Delta n_X(t) \approx n_g^{1s}$, under current experimental conditions, i.e., $n_g^{1s} \gg n_u^{1s}$. Here Δn_X thus quantitatively follows the $1s(g)$ exciton density, revealing, particularly, that the resonant photoexcitation generates $n_g^{1s} \sim 90\%$ of the total density, much larger than n_{eh} [inset, Fig. 3(c)].

With increasing off-resonant excitation the intraexcitonic $1s(g) \rightarrow 1s(u)$ responses reveal the complex many-particle state characterized by the coexistence and interplay between the robust quasi-1D excitons, both dark and bright, as well as dense $e-h$ plasma. Figs. 4(a)-(b) shows $\Delta\sigma_1^{\text{NT}}(\omega)$ and $\Delta\epsilon_1^{\text{NT}}(\omega)$ for various pump fluences after 1.55 eV photoexcitation at $T=5$ K. The spectra at $\Delta\tau=0.5$ ps clearly exhibit the $\omega_{g \rightarrow u}^{1s}$ resonance, despite 100s of meV detuning away from the excitonic resonances, much faster than the 100s of ps formation

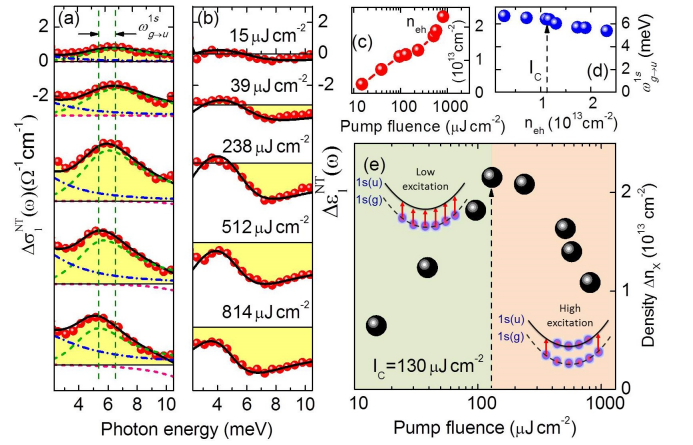


FIG. 4. (color online) (a)-(b) photo-induced $\Delta\sigma_1^{\text{NT}}(\omega)$ and $\Delta\epsilon_1^{\text{NT}}(\omega)$ changes (red dots) at various pump fluences after off-resonant excitation at 1.55 eV. $\Delta\tau=0.5$ ps and $T=5$ K. The model fitting (black lines) is divided into individual components (see text). The dashed lines indicate the shift of the $1s(g) \rightarrow 1s(u)$ peak positions. (c) The unbound $e-h$ density as a function of pump fluence. (d) The resonance peak as a function of unbound carrier density. (e) Fluence dependence of the exciton signal Δn_X , which is divided into two excitation regimes at $I_C \sim 130 \mu\text{J cm}^{-2}$ (dash arrow).

time observed in 2D/3D excitons under the off-resonant pumping [17]. The composite THz model (black lines) again consistently reproduces very well the experimental results, which are divided into individual components in the same manner as Fig. 2(a): the intraexcitonic $1s(g) \rightarrow 1s(u)$ (green lines) and unbound $e-h$ carriers (blue lines). Note the bleaching component of the 4 THz band (pink lines) [14] is added and *only* contributes at high pumping above $512 \mu\text{J cm}^{-2}$. Two salient features are visible with increasing pump fluence:

(1) The first feature is that the $\omega_{g \rightarrow u}^{1s}$ resonance in $\Delta\sigma_1^{\text{NT}}(\omega)$ shifts to lower frequency [Fig. 4(d)], illustrated by two dash lines in Fig. 4(a), $\sim 20\%$ change from 15 to $814 \mu\text{J cm}^{-2}$. We attribute this observation to the critical role of plasma-exciton interaction in the renormalization of the excitonic levels, considering the unbound $e-h$ density significantly increases in the off-resonance pumping, e.g., n_{eh} can reach $\sim 2.5 \times 10^{13} \text{ cm}^{-2}$, comparable to exciton density, shown in Figs. 4(c)(e). Note that the $\omega_{g \rightarrow u}^{1s}$ shift is not seen in the system of a predominant exciton population for the resonant pumping, shown in Fig. 3, which has larger exciton density but one order of magnitude smaller n_{eh} . This thus helps reconcile some seemingly contradictory results regarding the exciton stability in SWNT literature, e.g., photoluminescence spectra of dense excitons have shown no shift up to complete absorption saturation [4, 22], while ultra-violet pumping results in some slight excitonic shifts that have been attributed to free carrier generation [6].

(2) The second feature is that the exciton density Δn_X exhibits a distinct non-monotonic variation with increasing photoexcitation [Fig. 4(e)], which peaks at $I_C \sim 130 \mu\text{J cm}^{-2}$ followed by a significant decrease with further increasing pump fluence [23]. However, most interestingly, the intra-excitonic resonance $\omega_{g \rightarrow u}^{1s}$ exhibits *little shift or broadening* at I_C [$< 5\%$, dash arrow in Fig. 4(d)], indicating that there is *no obvious exciton ionization to unbound e-h plasma*. This appears to be fundamentally different from dense 2D and 3D excitons where the strong decrease of excitonic signals occurs *only* upon the ionization of excitons manifested by a significant shift, broadening, and ultimately the disappearance of the THz resonances. The quasi-1D many-body state in SWNTs reveal, instead, the evolution from a predominant dark exciton population in the $1s(g)$ to phase space filling of both the lowest dark and bright exciton pair states. Such crossover at I_C is illustrated by two shaded colors in Fig. 4(e): below I_C , photoexcited excitons primarily populate in the lowest lying dark state $1s(g)$ that leads to a rapid rise of Δn_X with increasing pump fluence; above I_C , photoexcited excitons have larger probability to populate the $1s(u)$ state rather than the $1s(g)$ ground state, due to electronic heating of the many-body systems, which is responsible for the reduction of the $\omega_{g \rightarrow u}^{1s}$ resonance via Pauli blocking of the transition [23]. This many-exciton state is stable against high density ionization since the $1s(g)/1s(u)$ pairs are protected by the symmetry and strong correlation, well-isolated from higher lying np exciton levels ($n > 2$) and continuum ($> 200 \text{ meV}$) [1, 2, 5].

In conclusion, we provide the first insights into the chirality-specific THz response of dark $e-h$ pair correlation and dynamics in SWNTs. The ultrafast intra-excitonic probe of the dark excitons, being independent of ground state symmetry and momentum conservation restrictions, allows to reveal the unique evolution of the quasi-1D many-exciton system in the highly non-equilibrium state and in the presence of dense $e-h$ plasma. This may evolve into a benchmark approach for quantitative exciton management in SWNT-based device development, and motivates for fundamental quantum phase discovery of excitons [13] and other strongly correlated excitations [24].

This work was supported by the National Science Foundation under award DMR-1055352.

*Corresponding author.

jwang@iastate.edu; jwang@ameslab.gov

†Present address: Ming Hsieh Department of Electrical Engineering, University of Southern California, 3737 Watt Way, Los Angeles, CA 90089-0271

- [2] J. Maultzsch, *et al.*, *Phys. Rev. B* **72**, 241402(R) (2005).
- [3] Y. Z. Ma, L. Valkunas, S. L. Dexheimer, S. M. Bachilo, and G. R. Fleming, *Phys. Rev. Lett.* **94**, 157402 (2005).
- [4] G. N. Ostojic *et al.*, *Phys. Rev. Lett.* **94**, 097401 (2005).
- [5] J. Wang, M. W. Graham, Y. Ma, G. R. Fleming, and R. A. Kaindl, *Phys. Rev. Lett.* **104**, 177401 (2010).
- [6] J. J. Crochet *et al.*, *Phys. Rev. Lett.* **107**, 257402 (2011).
- [7] H. Zhao, and S. Mazumdar, *Phys. Rev. Lett.* **93**, 157402 (2004).
- [8] V. Perebeinos, J. Tersoff, and P. Avouris, *Nano Lett.* **5**, 2495 (2005).
- [9] See, for example, J. Kono, R. J. Nicholas and S. Roche, *Topics in Applied Physics* **111**, 393 (2008).
- [10] R. Matsunaga, K. Matsuda, and Y. Kanemitsu, *Phys. Rev. Lett.* **101**, 147404 (2008).
- [11] O. N. Torrens, M. Zheng, and J. M. Kikkawa, *Phys. Rev. Lett.* **101**, 157401 (2008).
- [12] F. Xia, M. Steiner, Y. Lin, and P. Avouris, *Nat. Nanotech.* **3**, 609 (2008).
- [13] L. V. Butov, A. C. Gossard, and D. S. Chemla, *Nature* **418**, 751 (2002).
- [14] T. Kamprath *et al.*, *Phys. Rev. Lett.* **101**, 267403 (2008).
- [15] X. Xu, *et al.*, *J. Phys. Chem. C* **113**, 18106 (2009).
- [16] A. Ugawa, A. G. Rinzler, and D. B. Tanner, *Phys. Rev. B* **60**, R11305 (1999).
- [17] R. Huber, R. A. Kaindl, B. A. Schmid, and D. S. Chemla, *Phys. Rev. B* **72**, 161314(R) (2005); R. A. Kaindl, D. Hägele, M. A. Carnahan, R. Lövenich, and D. S. Chemla, *Nature* **423**, 734 (2003).
- [18] T. Ogawa, S. Watanabe, N. Minami, and R. Shimano, *Appl. Phys. Lett.* **97**, 041111 (2010).
- [19] I. Chatzakis, *et al.*, *Phys. Rev. B* **86**, 125110 (2012); L. Luo, *et al.*, *Nat. Commun.* **5**, 3055 (2014).
- [20] A. Jorio *et al.*, *Phys. Rev. B* **71**, 075401 (2005).
- [21] C. Manzoni *et al.*, *Phys. Rev. Lett.* **94**, 207401 (2005).
- [22] Y. Murakami, and J. Kono, *Phys. Rev. Lett.* **102**, 037401 (2009).
- [23] The same non-monotonic fluence dependence of the $\omega_{g \rightarrow u}^{1s}$ resonance is also observed with resonant E_{22} photoexcitation, which can be similarly understood.
- [24] T. Li, *et al.*, *Nature* **496**, 69 (2013); A. Patz, *et al.*, *Nat. Commun.* **5**, 3229 (2014); T. Li, *et al.*, *Phys. Rev. Lett.* **108**, 167401 (2012)

[1] F. Wang, G. Dukovic, L. E. Brus, and T. F. Heinz, *Science* **308**, 838 (2005).